HHS Public Access

Author manuscript

Science. Author manuscript; available in PMC 2019 July 30.

Published in final edited form as:

Science. 2019 May 10; 364(6440): 566–570. doi:10.1126/science.aav2572.

Particulate methane monooxygenase contains only mononuclear copper centers

Matthew O. Ross[1,2], **Fraser MacMillan**[3], **Jingzhou Wang**[4,5], **Alex Nisthal**[4,5,*], **Thomas J. Lawton**[1,2,†], **Barry D. Olafson**[6], **Stephen L. Mayo**[4,5], **Amy C. Rosenzweig**[1,2,‡], **Brian M. Hoffman**[1,2,‡]

[1]Department of Molecular Biosciences, Northwestern University, 2205 Tech Drive, Evanston, IL 60208, USA.

[2]Department of Chemistry, Northwestern University, 2145 Sheridan Road, Evanston, IL 60208, USA.

[3]Henry Wellcome Unit for Biological Electron Paramagnetic Resonance Spectroscopy, School of Chemistry, University of East Anglia, Norwich NR4 7TJ, UK.

[4]Division of Biology, California Institute of Technology, MC 114-96, 1200 East California Boulevard, Pasadena, CA 91125, USA.

[5]Division of Chemistry and Chemical Engineering, California Institute of Technology, MC 114-96, 1200 East California Boulevard, Pasadena, CA 91125, USA.

[6]Protabit, 1010 E. Union Street, Suite 110, Pasadena, CA 91106, USA.

Abstract

Bacteria that oxidize methane to methanol are central to mitigating emissions of methane, a potent greenhouse gas. The nature of the copper active site in the primary metabolic enzyme of these bacteria, particulate methane monooxygenase (pMMO), has been controversial owing to seemingly contradictory biochemical, spectroscopic, and crystallographic results. We present biochemical and electron paramagnetic resonance spectroscopic characterization most consistent with two monocopper sites within pMMO: one in the soluble PmoB subunit at the previously

‡Corresponding author. amyr@northwestern.edu (A.C.R.); bmh@northwestern.edu (B.M.H.).
*Present address: Xencor, 111 W. Lemon Avenue, Monrovia, CA 91016, USA.
†Present address: Johns Hopkins Applied Physics Laboratory, 11100 Johns Hopkins Road, Laurel, MD 20723, USA.

Author contributions: M.O.R, F.M., A.N., T.J.L., B.D.O, S.L.M., A.C.R., and B.M.H. designed experiments. M.O.R., F.M., J.W., and A.N. carried out experiments. M.O.R, A.C.R., and B.M.H. wrote the manuscript.

Competing interests: A patent related to this work has been issued: A. C. Rosenzweig, T. J. Lawton, A. Nisthal, J. S. Kostecki, H. K. Privett, F. Lee, B. Olafson, A. D. Dousis, “Engineered recombinant enzymes for methane oxidation” U.S. patent US9896700B2. B.D.O. is a cofounder and the CEO of Protabit, a for-profit company that develops and markets software for protein engineering and computational protein design. S.L.M. is a cofounder of Protabit.

Data and materials availability: All data are available in the manuscript or the supplementary materials.

SUPPLEMENTARY MATERIALS

science.sciencemag.org/content/364/6440/566/suppl/DC1
Materials and Methods
Supplementary Text
Figs. S1 to S16
Tables S1 to S3
References (*49*–*68*)

assigned active site (Cu_B) and one ~2 nanometers away in the membrane-bound PmoC subunit (Cu_C). On the basis of these results, we propose that a monocopper site is able to catalyze methane oxidation in pMMO.

Methane is both a potent greenhouse gas and a readily available energy source (1–3). Methanotrophic bacteria use enzymes called methane monooxygenases (MMOs) to activate dioxygen and break a 105 kcal/mol C–H bond in methane to produce methanol at ambient pressure and temperature(1). By contrast, current industrial catalysis processes for this reaction require tremendous pressure and high temperature (>1000 K). Understanding how enzymes catalyze this reaction is critical to the development of catalysts that function at moderate conditions (4–8).

The most common MMO is the membrane-bound, copper-dependent particulate enzyme (pMMO) (9). Multiple pMMO crystal structures reveal a trimeric assembly of protomers, each comprising two predominantly transmembrane subunits (PmoA and PmoC) and one transmembrane subunit with a large periplasmic domain (PmoB) (Fig. 1A) (10–13). Three copper-binding sites have been detected in the pMMO structures, (i) A monocopper site, denoted as the bis-His site, is ligated by His^{48} and His^{72} (fig. S1). However, His^{48} is not conserved, and this site is observed only in the *Methylococcus capsidatus* (Bath) pMMO structure (10), so it is not believed to play a critical role in catalysis (14). (ii) All structures contain a site denoted Cu_B, in which copper is coordinated by the amino-terminal histidine of PmoB (His^{33}) as well as His^{137} and His^{139} [Fig. 1A, *M. capsulatus* (Bath) numbering]. On the basis of extended x-ray absorption fine structure (EXAFS) data, this site was initially modeled as dicopper in some (10,11, 15), but not all (11–13), structures, with a later quantum refinement study supporting the monocopper assignment (16). LUntil now, it remained unclear whether the monocopper Cu_B site in the crystal structures is due to copper loss during the purification/crystallization process or whether Cu_B is actually a monocopper center, (iii) Last, a copper ion is found in the PmoC subunit coordinated by residues Asp^{156}, His^{160}, and His^{173}(12).

The nuclearity, ligation, and location of the pMMO copper active site have been difficult to assign. The pMMO isolation and purification procedure has been suggested to result in loss or alteration of the essential metallocofactor, which is consistent with the substantially lower activity of pMMO after isolating the membranes from the organism (≲17% of that in vivo) (9,13). Variable metal content and enzymatic activity not having been demonstrated in crystals also call into question the physiological and catalytic relevance of the metallocofactors observed in crystal structures. Catalysis has been proposed to occur at three different types of multinuclear center, two of which have been dismissed: a tricopper site in PmoA (17–19), which is neither observed crystallographically nor by multiple investigators (including ourselves) with electron paramagnetic resonance (EPR) spectroscopy (20–25), and a diiron center at the PmoC metal-binding site (26), which is ruled out by the observation that copper, not iron, restores activity of metal-depleted pMMO (27). The third such proposal is that the active site is a dicopper Cu_B, located at the amino terminus of PmoB (27). This report addresses the Cu nuclearity in pMMO and shows that pMMO only contains two distinct monocopper sites. A detailed discussion and reconciliation of prior

experiments (which were interpreted in terms of pMMO containing a dicopper center) with the present conclusion is provided in the supplementary materials.

To circumvent any complications arising from loss of copper cofactors through enzyme purification, we probed the pMMO Cu(II) sites in whole cells of *M capsulatus* (Bath) grown on ^{15}N and ^{63}Cu with EPR spectroscopy. Under copper-replete conditions, pMMO is highly expressed [~20% of total protein (26)]. Therefore, any Cu(II) sites within the protein should be present in such high quantity as to dominate the in vivo EPR spectrum. Indeed, prior EPR spectra of wholecell methanotroph samples exhibited a type 2 Cu(II) EPR signal with four N equatorial ligands that was attributed to pMMO-bound Cu(II) on the basis of the high Cu(II) concentration and similarity to the EPR spectrum of isolated methanotroph membranes (18,20,28). As a precursor to advanced spectroscopic characterization of the pMMO Cu(II), we first confirmed that we too observed this type 2 Cu(II) EPR signal, with four N equatorial ligands [as indicated by a five-line ^{15}N hyperfine splitting of the low-field g_1 Cu(II) hyperfine transition (fig. S2)], in the whole-cell (Vivo-pMMO) EPR spectrum of ^{15}N, ^{63}Cu-enriched *M. capsulatus* (Bath) (g = [2.242,2.068, 2.035]; ^{63}Cu hyperfine splitting A_1 = 570 MHz or 190 × 10^{-4} cm^{-1}) (Fig. 1 and fig. S2). The ratio of $g_1/A_1(cm^{-1})$ = 118 cm indicates a highly planar equatorial Cu coordination (29–31).

We characterized the nitrogenous ligands of this Cu(II) species with electron nuclear double resonance (ENDOR) spectroscopy. ^{15}N Davies ENDOR spectra collected near g_1 exhibited strongly coupled^{15}N resonances corresponding to two similar directly coordinated Cu(II) ligands [$|A_1(^{15}N)|$~48,53 MHz] (Fig. 2A); Gaussian fitting and quantitation of the resonances indicated that the ν_+ peak with the larger coupling is three times more intense than the other ν_+ peak (Fig. 2B and tables S1 and S2). The near equivalence of these couplings combined with the quantitation is evidence for a Cu(II) site with four (determined by the 3:1 intensity ratio) equatorial ^{15}N ligands bound in a square plane (32). ^{15}N Doan/ReMims ENDOR spectra collected near also exhibit weakly coupled ^{15}N resonances from the remote (noncoordinated) ^{15}N of histidyl imidazoles bound to Cu(II) ($|A_1(^{15}N)|$~1.7, 2.3 MHz) (Fig. 2A) (33) in a 1:2 intensity ratio (Fig. 2B and tables S1 and S2). Thus, of the four N ligands defined by the ^{15}N Davies ENDOR, three are histidyl imidazole side chains. Consistent with this assignment, ^{1}H Davies ENDOR measurements showed nonexchangeable signals with couplings of A_2 ~ 4.5 and 2.5 MHz, which is characteristic of the ring protons of Cu(II)-bound histidyl imidazole (fig. S3 and table S1) (34). Additional broad, exchangeable ^{1}H signals with couplings $|A_1| \sim |A_2| \sim 10$ MHz are as expected for protons of $-NH_2$ coordinated to Cu(II) (fig. S3 and table S1) (34).

To assign the location of this Cu(II) species, we examined the histidine residues in all pMMO crystal structures, looking for sites where three imidazoles and an $-NH_2$ could simultaneously coordinate a Cu(II). The only location that can supply this spectroscopically defined ligand set is the Cu_B site (Fig. 1 and fig. S4), which provides three imidazole nitrogens from His^{33}, His^{137}, and His^{139} as well as the $-NH_2$ of His^{33}. The correspondence between this ligand assemblage and the EPR/ENDOR-defined ligation strongly supports assignment of Cu_B as a monocopper site.

To characterize any pMMO copper sites that might be maintained in vivo in the reduced Cu(I) state, we allowed them to air oxidize by solubilizing and purifying *M. capsulatus* (Bath) pMMO with size exclusion chromatography (Purified-pMMO). The Cu_B(II) signal persisted in Purified-pMMO, but another Cu(II) signal appeared, denoted Cu_c (g = [2.30,2.07,2.05]; ^{63}Cu hyperfine splitting A_1 = 440 MHz or 147 × 10^{-4} cm^{-1}) (Fig. 2), as previously observed in purified pMMO EPR samples (13,24). The larger Cu_c(II) g_1/A_1 = 156 cm is characteristic of a distorted (flattened) tetrahedral geometry (35,36). In support of the conclusion that pMMO houses only monocopper centers, we have also found that an optical spectrum previously proposed to result from a dicopper center (37) is instead associated with a product of O_2 or H_2O_2 oxidation of ascorbate in the presence of methanol and copper (fig. S5 and supplementary text).

Reduction of Purified-pMMO (Reduced/Purified pMMO) effectively eliminated the Cu_c(II) EPR signal, leaving a Cu_B(II) signal virtually identical to that observed in vivo (Fig. 2), similar to previous reports of the reduction of pMMO localized in methanotroph membranes (18, 38), and with unchanged ^{15}N ENDOR responses (Fig. 2), confirming that the Cu_B(II) site is unchanged during purification. The nonexchangeable signals from the imidazole ring protons and the exchangeable signals from protons attributed to $-NH_2$ (fig. S3B) are also unchanged. We farther addressed the four-N ligation of Cu_B by EPR/ENDOR characterization of Reduced/Purified-pMMO incubated with $H_2{}^{17}O$. The characteristic ^{17}O ENDOR response of an equatorially coordinated H_xO is absent, showing that Cu_B does not have such a ligand (fig. S6). The experiments did exhibit the ^{17}O signal characteristic of an axial $H_x{}^{17}O$ on Cu_B, however, meaning that the geometry of Cu_B(II) is best described as square pyramidal.

To determine the location of the Cu_c(II) site, we measured Cu(II)-Cu(II) distances in Purified-pMMO with double electron-electron resonance (DEER) spectroscopy. The background-corrected DEER dipolar evolution for Purified-pMMO and corresponding Cu(II)-Cu(II) distance distribution obtained through Fourier transformation (39) are shown in Fig. 3. The transform of this 2.5-μs dipolar evolution can be considered robust for distances (d)of $2 \lesssim d \lesssim 5$ nm. There are two peaks in the distance distribution: a major peak at a distance of 4.5 nm and a minor peak at 2.8 nm. The 2.8-nm peak is very weak and is extremely variable in intensity depending on the procedure used to analyze the time wave (fig. S7), whereas the 4.5-nm distance is robust, and indeed its counterpart can be clearly seen as the sinusoidal modulation of the time-evolution trace. Thus, we consider the shorter distance peak to be an artifact of the data processing.

We compared the 4.5-nm distance with the Cu-Cu distances in the *M. capsulatus* (Bath) pMMO crystal structure, which contains two metal-binding sites besides the Cu_B site: the bis-His site in PmoB (fig. S1) and the PmoC metal binding site (Fig. 1). If the Cu_c(II) EPR signal corresponded to the bis-His site, a second robust Cu-Cu distance of ~3.2 nm (Cu_c to Cu_c) would be expected as well as the ~4.4-nm distance (in-terprotomer Cu_B to Cu_c), contrary to observation. However, assignment of Cu_c(II) to the PmoC site predicts a single Cu-Cu distance of −4.4 nm (Cu_c to Cu_c) (Fig. 3C), which is in agreement with the data. The intraprotomer ~2-nm Cu_B-to-Cuc distance distribution is not observed, presumably because it is too close to the minimum distance that can be resolved. Overall, the distance

measurements indicate that Cue is not located in the bis-His site and instead is located in the PmoC metal binding site. There is no evidence of Cu(II) in the bis-His site in this sample or in any other structures [including one in which both histidines are present (13)], implying that this site may have been adventitious in the initial structure (10). This assignment is supported by ^{15}N ENDOR measurements on Purified-pMMO (Fig. 3), which are consistent with the PmoC Cu_c ligand assemblage depicted in Fig. 1. ^{1}H and ^{17}O ENDOR further indicate that Cu_c contains a H_xO ligand (figs. S3 and S6), as modeled in two pMMO crystal structures (11,12).

The characterization of these two monocopper sites in pMMO reopens the question of the identity of the catalytic site. The mononuclear Cu_B site exhibits saturated equatorial coordination, with strongly bound N-ligands, and thus is unlikely to undergo O_2-binding/activation without alteration. However, addition of nitrite [a known inhibitor of methane oxidation (40,41)] perturbs the Cu_c(II) EPR signal (fig. S8A), and ENDOR characterization of pMMO after addition of ^{15}N-nitrite revealed a small ^{15}N hyperfine coupling (A ~ 0.3 MHz), which is consistent with NO_2^- bound to Cu(II) through the oxygen(s) (fig. S8B) (42). This observation, combined with Verrucomicrobial pMMOs possessing none of the Cu_B-ligating amino acids (43), prompted us to reinvestigate the activity of the spmoB protein. This recombinantly expressed construct comprises the soluble portion of the *M. capsulatus* (Bath) PmoB subunit and is a model for native PmoB copper binding. It was reported to exhibit methane oxidation activities 1 to 10% that of pMMO (24,27), the only direct evidence identifying Cu_B as the active site.

To probe Cu_B reactivity in a more stable protein platform, we generated several fusion constructs of spmoB (fig. S9) that did not require refolding after expression [unlike spmoB, which expresses into inclusion bodies (27)]. One of these constructs assembled a Cu_B(II) site very similar to Cu_B(II) of pMMO by EPR (fig. S10A), unlike spmoB, which exhibits a different EPR spectrum (24). We tested the new constructs and the original spmoB for activity (figs. S10B and S11). These reaction mixtures produced ^{13}C-methanol when assayed for ^{13}C-methane oxidation. However, the amount of ^{13}C-methanol produced was not affected by mutating the Cu_B site in the soluble spmoB construct; by altering the temperature, reaction time, protein concentration; or by using an unrelated copper enzyme incapable of oxidizing methane (fig. S11, C to E). The activity observed in these assays is instead attributed to the ability of duroquinol to reduce O_2 and generate H_2O_2. H_2O_2 in turn can produce $OH^\bullet$ through autolysis and through Fenton and Haber-Weiss chemistry (44–47), which then oxidizes methane. These experiments indicate that Cu_B in spmoB does not catalyze methane oxidation, thus eliminating the grounds for proposing Cu_B as the pMMO active site.

Instead, there is evidence that Cu_c, located in the site illustrated in Fig. 1, may be the site of O_2 binding and methane oxidation. Such a model would be consistent with the suggested presence of a displaceable solvent ligand on Cu_c, as needed for O_2-binding/activation, binding of the nitrite inhibitor to Cu_c, and the absence of the Cu_B site in the Verrucomicrobial pMMOs. Last, mutation of any Cu_c ligand in a pMMO homolog from *Mycobacterium* NBB4 (hydrocarbon monooxygenase) resulted in complete loss of activity (48). Cu_c is thus inferred to be the active site of hydrocarbon substrate binding and

oxidation, but Cu_B nonetheless is important. Replacement of a Cu_B ligand in the homolog diminished overall activity significantly (by 80%), but the variant's affinity for alkane substrate was within error of wild type for two of the three alkanes assayed (48), indicating that Cu_B does play a functional role, even though it is not the site of hydrocarbon substrate binding and oxidation.

Supplementary Material

Refer to Web version on PubMed Central for supplementary material.

ACKNOWLEDGMENTS

We thank G. E. Cutsail III, M. A. Culpepper, and H. W. Pinkett for helpful discussions as well as an anonymous reviewer for the expert analysis of the Gaussian fitting and providing above and beyond effort.

Funding: This work was supported by NIH grants GM118035 (A.C.R.), GM111097 (B.M.H.), and 5T32GM008382 (M.O.R.) and NSF grant 1534743 (S.L.M., B.D.O., and A.C.R.). F.M. was supported by a Royal Society Wolfson Research Merit Award.

REFERENCES AND NOTES

1. Ross MO, Rosenzweig AC, J. Biol. Inorg. Chem 22, 307–319 (2017). [PubMed: 27878395]
2. Brandt AR et al., Science 343, 733–735 (2014). [PubMed: 24531957]
3. Environmental Protection Agency (EPA), Inventory of U.S. greenhouse gas emissions and sinks: 1990-2015 (EPA, 2017).
4. Fei Q et al., Biotechnol. Adv 32, 596–614 (2014). [PubMed: 24726715]
5. Horn R, Schlögl R, Catal. Lett 145, 23–39 (2015).
6. Snyder BER, Bols ML, Schoonheydt RA, Sels BF, Solomon EI, Chem. Rev 118, 2718–2768 (2018). [PubMed: 29256242]
7. Khan MS, Park JH, Chaniago YD, Lee M, Energy Procedia 61, 599–602 (2014).
8. Gao J et al., Science 348, 686–690 (2015). [PubMed: 25858978]
9. Lawton TJ, Rosenzweig AC, J. Am. Chem. Soc 138, 9327–9340 (2016). [PubMed: 27366961]
10. Lieberman RL, Rosenzweig AC, Nature 434, 177–182 (2005). [PubMed: 15674245]
11. Smith SM et al., Biochemistry 50, 10231–10240 (2011). [PubMed: 22013879]
12. Sirajuddin S et al., J. Biol. Chem 289, 21782–21794 (2014). [PubMed: 24942740]
13. Ro SY et al., J. Biol. Chem 293, 10457–10465 (2018). [PubMed: 29739854]
14. Balasubramanian R, Rosenzweig AC, Acc. Chem. Res 40, 573–580 (2007). [PubMed: 17444606]
15. Hakemian AS et al., Biochemistry 47, 6793–6801 (2008). [PubMed: 18540635]
16. Cao L, Caldararu O, Rosenzweig AC, Ryde U, Angew. Chem. Int. Ed 57, 162–166 (2018).
17. Wang VCC et al., Chem. Rev 117, 8574–8621 (2017). [PubMed: 28206744]
18. Nguyen HH et al., J. Biol. Chem 269, 14995–15005 (1994). [PubMed: 8195135]
19. Chan SI et al., Angew. Chem. Int. Ed 46, 1992–1994 (2007).
20. Yuan H, Collins MLP, Antholine WE, J. Am. Chem. Soc 119, 5073–5074 (1997).
21. Choi DW et al., Microbiology 151, 3417–3426 (2005). [PubMed: 16207923]
22. Basu P, Katterle B, Andersson KK, Dalton H, Biochem. J 369, 417–427 (2003). [PubMed: 12379148]
23. Lieberman RL et al., Proc. Natl. Acad. Sei. U.S.A. 100, 3820–3825 (2003).
24. Culpepper MA, Cutsail GE III, Gunderson WA, Hoffman BM, Rosenzweig AC, J. Am. Chem. Soc 136, 11767–11775 (2014). [PubMed: 25059917]
25. Zahn JA, DiSpirito AA, J. Bacteriol 178, 1018–1029 (1996). [PubMed: 8576034]
26. Martinho M et al., J. Am. Chem. Soc 129, 15783–15785 (2007). [PubMed: 18052283]

27. Balasubramanian R et al., Nature 465, 115–119 (2010). [PubMed: 20410881]
28. Lemos SS, Perille Collins ML, Eaton SS, Eaton GR, Antholine WE, Biophys. J 79, 1085–1094 (2000). [PubMed: 10920038]
29. Sakaguchi U, Addison AW, J. Chem. Soc 600–608 (1979).
30. Pogni R, Baratto MC, Diaz A, Basosi R, J. Inorg. Biochem 79, 333–337 (2000). [PubMed: 10830885]
31. Patel RN et al., Inorg. Chim. Acta 362, 4891–4898 (2009).
32. Iwaizumi M, Kudo T, Kita S, Inorg. Chem 25, 1546–1550 (1986).
33. Dicus MM et al., J. Am. Chem. Soc 132, 2037–2049 (2010). [PubMed: 20099820]
34. Manikandan P, Epel B, Goldfarb D, Inorg. Chem 40, 781–787 (2001). [PubMed: 11225123]
35. Yokoi H, Bull. Chem. Soc. Jpn 47, 3037–3040 (1974).
36. Cheeseman TP, Hall D, Waters TN, J. Chem. Soc. A 1966, 685–693 (1966).
37. Culpepper MA, Cutsail III GE, Hoffman BM, Rosenzweig AC, J. Am. Chem. Soc 134, 7640–7643 (2012). [PubMed: 22540911]
38. Yuan H, Collins ML, Antholine WE, J. Inorg. Biochem 72, 179–185 (1998). [PubMed: 10065536]
39. Jeschke G et al., Appl. Magn. Reson 30, 473–498 (2006).
40. Nyerges G, Stein LY, FEMS Microbiol. Lett 297, 131–136 (2009). [PubMed: 19566684]
41. Stein LY, Arp DJ, Appl. Environ. Microbiol 64, 4098–4102 (1998). [PubMed: 9758853]
42. Fittipaldi M et al., Biochemistry 44, 15193–15202 (2005). [PubMed: 16285722]
43. Op den Camp HJ et al., Environ. Microbiol. Rep 1, 293–306 (2009). [PubMed: 23765882]
44. White CC, Chain RK, Malkin R, Biochim. Biophys. Acta 502, 127–137 (1978). [PubMed: 638137]
45. Taylor CE, Prepr. Pap.-Am. Chem. Soc. Div. Fuel Chem. 48, 876 (2003).
46. Cadenas E, Boveris A, Ragan CI, Stoppani AOM, Arch. Biochem. Biophys 180, 248–257 (1977). [PubMed: 195520]
47. Ikai H et al., Antimicrob. Agents Chemother. 54, 5086–5091 (2010). [PubMed: 20921319]
48. Liew EF, Tong D, Coleman NV, Holmes AJ, Microbiology 160, 1267–1277 (2014). [PubMed: 24682027]

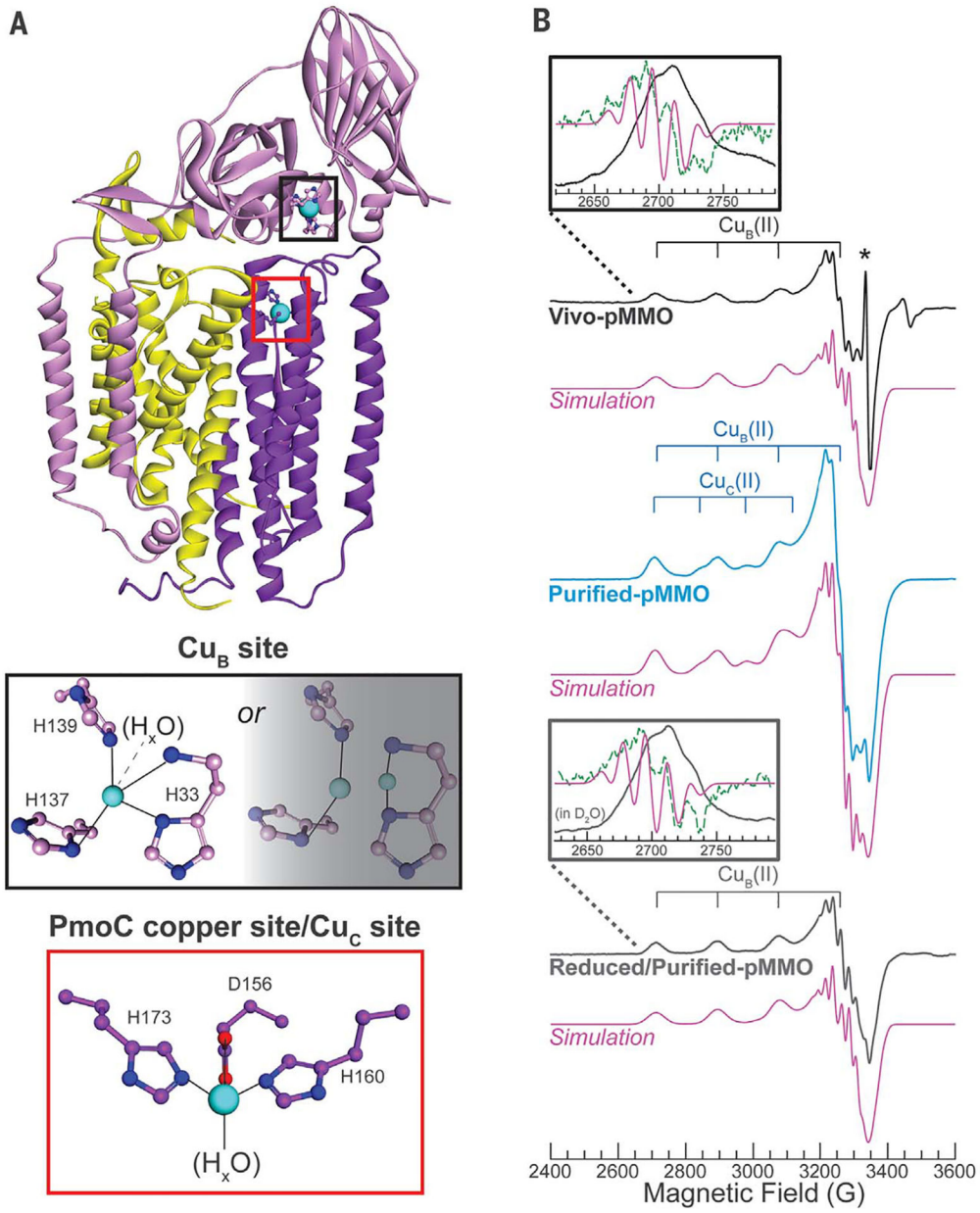

Fig. 1. Structure of one pMMO protomer as well as X-band continuous wave (CW) EPR of Vivo-[showing CuB(II)], Purified-[showing CuB(II) and Cuc(II)], and Reduced/Purified-pMMO [showing CuB(II)].

(**A**) (Top) Single protomer from the *M. capsulatus* (Bath) pMMO crystal structure (DOI: 10.2210/pdb3rgb/pdb) (11), showing PmoA (yellow), PmoB (pink), PmoC (purple), Cu (cyan), N (blue), and O (red) atoms. (Middle) The Cu_B site modeled as monocopper and dicopper. (Bottom) The PmoC metal site, which we have now determined to be the Cu_C site, occupied with copper. (**B**) EPR spectra with simulations of the Cu_B(II) (Vivo- and Reduced/Purified-pMMO) and Cu_B(II) plus 0.32 equivalents Cu_C(II) (Purified-pMMO) shown below each spectrum. (Insets) Lowest-field Cu hyperfine transition with computed second derivative (green dotted line) and second derivative of the simulation (pink solid line). Asterisk denotes an organic radical species in Vivo-pMMO. This radical is not present in

Purified- or Reduced/Purified-pMMO. In the Reduced/Purified-pMMO (inset), the two lowest field ^{15}N hyperfine lines are unresolved, likely because of a small amount of $Cu_C(II)$. Spectra and simulation parameters are listed in table S1, and collection conditions are provided in the supplementary materials. Rapid-passage Q-band absorption-display CW EPR spectra are shown in fig. S12. Unless otherwise noted, the concentrations of all EPR/ENDOR samples of Purified- or Reduced/Purified-pMMO were 300 to 500 μM. All pMMO spectra shown in the main text were measured on ^{63}Cu, ^{15}N-labeled pMMO samples.

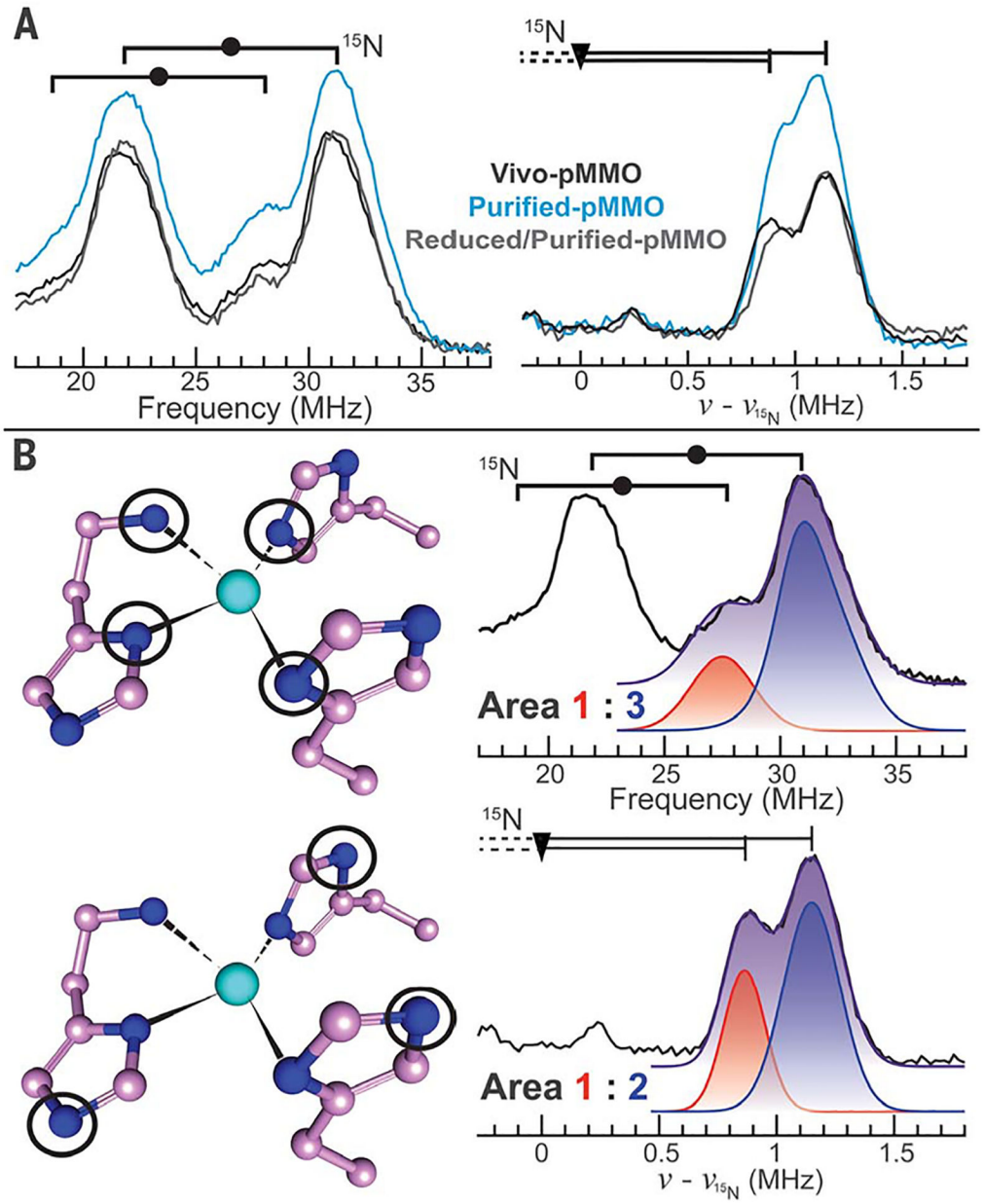

Fig. 2. Characterization of Cub(II) and Cuc(II) ^{15}N ligation with ENDOR.

(**A**) Q-band pulsed ENDOR measurements collected at $g_1$for (left) strongly and (right) weakly coupled ^{15}N nuclei, using Davies and Doan/ReMims ENDOR, respectively (Left) Goalpost widths indicate twice the ^{15}N Larmor frequency ν(^{15}N), and the filled circles define half the hyperfine coupling magnitude (|*A*/2|). (Right) The triangle defines ν(^{15}N), and the distance from triangle to vertical line equals |*A*/2|. (**B**)(Left) Circled nitrogen atoms produce the observed ENDOR responses to the right of each Cu_B site. (Right) Overlay of Vivo-pMMO experimental spectra with individual (red and blue) and summed (purple) Gaussian functions used to quantitate ^{15}N resonance peaks. Parameters are listed in tables S1 and S2, and collection conditions are provided in the supplementary materials. Although

only the v_+ peak is shown for the Vivo-pMMO weakly coupled ^{15}N ENDOR response, both v_- and v_+ are shown in fig. S13.

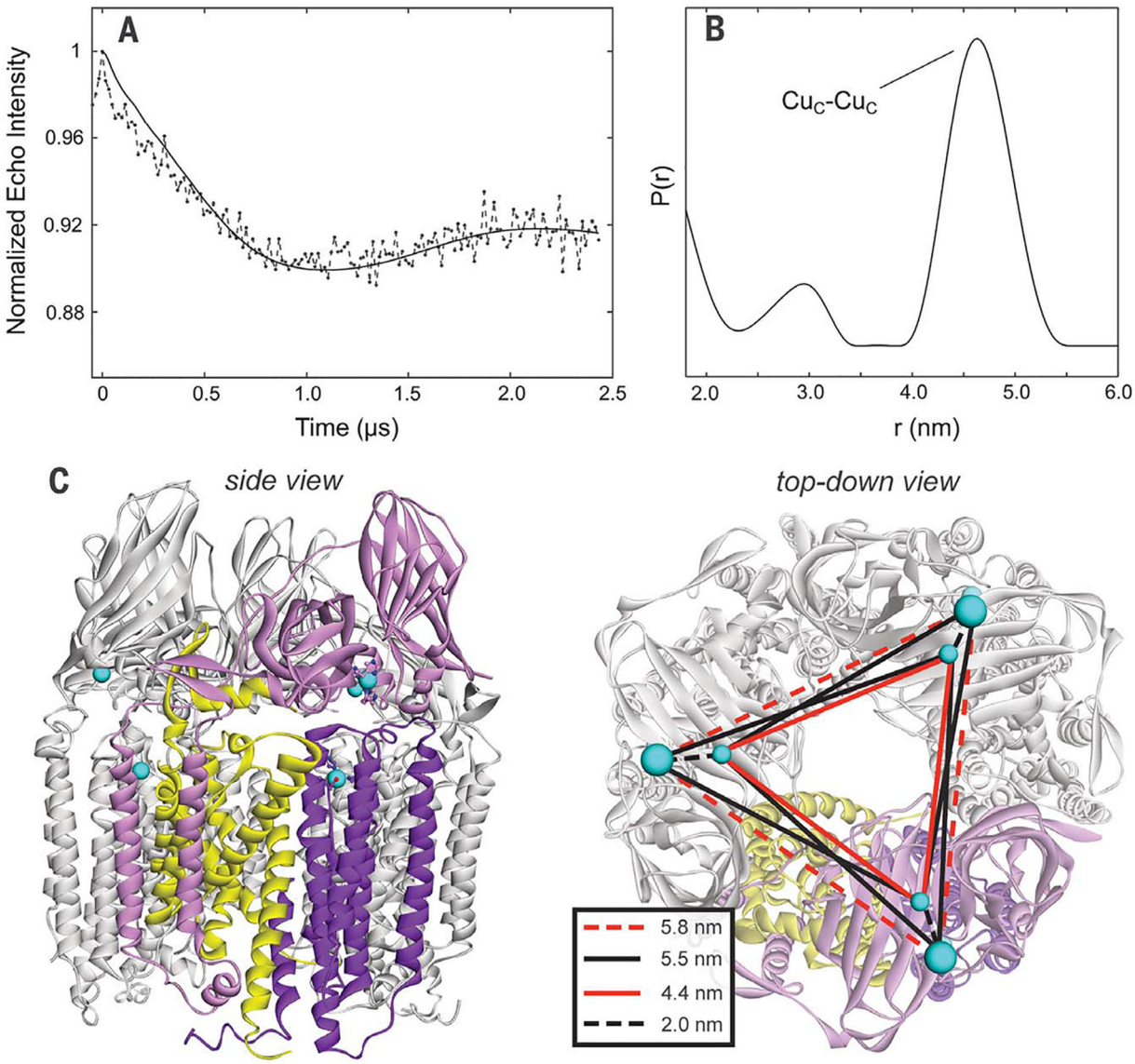

Fig. 3. Purified-pMMO Cu(II)-Cu(II) four pulse DEER distance measurements.

(**A**) Normalized first-order homogeneous background decay-corrected dipolar evolution (solid line is a fitting of the dipolar evolution using DeerAnalysis2016). (**B**) Cu(II)–Cu(II) distance distributions calculated by using DeerAnalysis 2016. The measured Cu(II)–Cu(II) distance (4.5 nm) is consistent with the distances expected for Cuc(II) in the PmoC variable metal site and excludes the presence of Cu(II) in the bis-His site; if Cu_c(II) was located in the bis-His site, a 3.2-nm Cu(II)—Cu(II) distance would be predicted (fig. S1). (**C**) Crystal structure of the *M. capsulatus* (Bath) pMMO trimer with same coloring as Fig. 1 (except two protomers are globally colored gray), and the various predicted Cu-Cu distances (inset).